

Article

Investigation of Pharmaceutical Importance of 2H-Pyran-2-One Analogues via Computational Approaches

Samata E. Shetgaonkar ¹, Shiva Prasad Kollur ^{2,*}, Renjith Raveendran Pillai ^{3,4}, Karthick Thangavel ⁵, Sanja J. Armaković ⁶, Stevan Armaković ⁷, Chandan Shivamallu ⁸, Raghavendra G. Amachawadi ⁹, Asad Syed ¹⁰, Abdallah M. Elgorban ¹⁰, Ali H. Bahkali ¹⁰ and Fateh V Singh ^{1,*}

- ¹ Chemistry Division, Chennai Campus, School of Advanced Science, VIT University, Chennai 600127, Tamil Nadu, India; samatashetgaonkar@vit.ac.in
 - ² Department of Sciences, Amrita Vishwa Vidyapeetham, Mysuru Campus, Amrita School of Arts and Sciences, Mysuru 570026, Karnataka, India
 - ³ Department of Physics, T.K.M. College of Arts and Science, Karicode, Kollam 691005, Kerala, India; renjithkadavoor@tkmc.edu.in
 - ⁴ Central Polytechnic College, Vattiyoor kavu, Trivandrum, Tamil Nadu 600113, Kerala, India
 - ⁵ School of Electrical & Electronics Engineering, SASTRA Deemed University, Tirumalaisamudram, Thanjavur 613401, Tamil Nadu, India; karthick.t@sastra.edu.in
 - ⁶ Department of Chemistry, Biochemistry and Environmental Protection, Faculty of Sciences, University of Novi Sad, Trg D, Obradovića 3, 21000 Novi Sad, Serbia; sanja.armakovic@dh.uns.ac.rs
 - ⁷ Department of Physics, Faculty of Sciences, University of Novi Sad, Trg D, Obradovića 4, 21000 Novi Sad, Serbia; stevan.armakovic@df.uns.ac.rs
 - ⁸ Department of Biotechnology and Bioinformatics, School of Life Sciences, JSS Academy of Higher Education and Research, Mysuru 570015, Karnataka, India; chandans@jssuni.edu.in
 - ⁹ Department of Clinical Sciences, College of Veterinary Medicine, Kansas State University, Manhattan, KS 66506-5606, USA; agraghav@vet.k-state.edu
 - ¹⁰ Department of Botany and Microbiology, College of Science, King Saud University, P.O. Box 2455, Riyadh 11451, Saudi Arabia; assyed@ksu.edu.sa (A.S.); aelgorban@ksu.edu.sa (A.M.E.); abahkali@ksu.edu.sa (A.H.B.)
- * Correspondence: shivachemist@gmail.com or shivaprasad.k@my.amrita.edu (S.P.K.); fatehveer.singh@vit.ac.in (F.V.S.)



Citation: Shetgaonkar, S.E.; Kollur, S.P.; Pillai, R.R.; Thangavel, K.; Armaković, S.J.; Armaković, S.; Shivamallu, C.; Amachawadi, R.G.; Syed, A.; Elgorban, A.M.; et al. Investigation of Pharmaceutical Importance of 2H-Pyran-2-One Analogues via Computational Approaches. *Symmetry* **2021**, *13*, 1619. <https://doi.org/10.3390/sym13091619>

Academic Editor: Miroslav Ilijaš

Received: 6 July 2021

Accepted: 30 August 2021

Published: 3 September 2021

Publisher's Note: MDPI stays neutral with regard to jurisdictional claims in published maps and institutional affiliations.



Copyright: © 2021 by the authors. Licensee MDPI, Basel, Switzerland. This article is an open access article distributed under the terms and conditions of the Creative Commons Attribution (CC BY) license (<https://creativecommons.org/licenses/by/4.0/>).

Abstract: Highly functionalized spirocyclic ketals were synthesized through asymmetric oxidative spirocyclization via carbanion-induced ring transformation of 2H-pyran-2-ones with 1,4-cyclohexandione monoethyleneketal under alkaline conditions. Further acidic-hydrolysis of obtained spirocyclic ketals yields highly substituted 2-tetralone in good yield. Computational analysis based on the DFT calculations and MD simulations has been performed in order to predict and understand global and local reactivity properties of newly synthesized derivatives. DFT calculations covered fundamental reactivity descriptors such as molecular electrostatic potential and average local ionization energies. Nitrogen atom and benzene rings have been recognized as the most important molecular sites from these aspects. Additionally, to predict whether studied compounds are stable towards the autoxidation mechanism, we have also studied the bond dissociation energies for hydrogen abstraction and identified the derivative which might form potentially genotoxic impurities. Interactions with water, including both global and local aspects, have been covered thanks to the MD simulations and calculations of interaction energies with water, counting of formed hydrogen interactions, and radial distribution functions. MD simulations were also used to identify which excipient could be used together with these compounds, and it has been established that the polyvinylpyrrolidone polymer could be highly compatible with these compounds, from the aspect of calculated solubility parameters.

Keywords: tetralone; DFT calculations; MD simulations; MEP; bond dissociation

1. Introduction

A well-known aromatic bicyclic ketone derived from tetralin, 2-Tetralone, has been identified as an essential intermediate for the synthesis of natural products and biologically valuable compounds [1–4]. Moreover, tetralone-derived polyaromatic compounds with donor and acceptor groups exhibit amazing absorption and emission properties [5,6]. Further phenanthridine based fluorescent chemosensors have been designed for the detection of heavy metal ions such as Hg^{2+} and Ru^{+3} using β -tetralone as key precursor [7,8]. Additionally, dihydrophenanthrenes synthesized via ring transformation of 2H-pyran-2-ones with 2-tetralone under basic condition have been successfully utilized in fabricating blue, sky-blue, and green color light-emitting devices [9]. Apart from this, 2-tetralones are potential precursors for the construction of tetrahydronaphthalene-based naturally occurring and pharmacologically active molecules. Tetrahydronaphthalene-cored compounds are well known for their interesting anti-tumor [10], antimicrobial [11], antidepressant [12], and anti-inflammatory activities [13]. Idarubicin, an antileukemic glycoside [14], and (\pm) daunomycinone [15], a potent antibiotic with anticancer activity, are tetralin-cored drug molecules derived from 2-tetralones. Another interesting drug molecule, Nepinalone, synthesized by reacting 1-methyl-2-tetralone with 1-N-(2-chloroethyl)piperidine, is a compound exhibiting antitussive activity [16]. Furthermore, rotigotine is a dopamine agonist used in the treatment of Parkinson's disease [17] while treprostinil is used to treat pulmonary hypertension [18]. Thus, compounds of this type are potential candidates for the development of drug molecules for the treatment of different diseases related to the central nervous system (CNS). In view of the above important facts, a number of organic chemists are actively engaged in the asymmetric synthesis of spirocyclic skeletons having cyclohexane, cyclohexene, and cyclohexanone motifs.

In this work, a set of first principles and classical calculations have been performed in order to understand global and local reactivity properties of the as-synthesized molecules. Computational modelling of organic molecules with pharmaceutical potential has been recognized as one of the most important steps in the development of novel pharmaceutical products, due to its ability to predict important physical and chemical properties and, in this way, to accelerate the drug design process [19]. As evidenced by numerous publications, the combination of DFT calculations and MD simulations have been proven to be particularly useful for these purposes [20–24], which was a clear motivation for the application of these methods in this study as well.

2. Materials and Methods

2.1. General Procedure for the Synthesis of Functionalized Spirocyclic Ketals 7

To a 25 mL round bottom flask, containing 2H-pyran-2-one 5 (1.0 mmol, 1.0 equiv) and 1,4-cyclohexanedione monoethylene ketal 6 (1.2 mmol, 1.2 equiv), was added powdered KOH (1.2 mmol) in dry DMSO (3.0 mL) and the resulting reaction mixture was placed in an ultrasonic bath for 26 to 37 min for irradiation at room temperature. The course of the reaction completion was monitored by TLC and the spots were visualized under UV light. The reaction was quenched by the addition of ice-cold H_2O (10 mL) and the mixture was neutralized with dilute HCl, followed by extraction with EtOAc (3×10 mL) and the combined organic layer was dried over Na_2SO_4 , filtered, and evaporated under vacuum. The crude product obtained was then purified using column chromatographic technique using EtOAc/hexane (1:4) as the eluent. Finally, the desired products, ketals 7, were characterized by spectroscopic analysis.

2.2. General Procedure for the Synthesis of Functionalized 2-Tetralone 11

A solution of spirocyclic ketal 7 (0.25 mmol) in 4% ethanolic-HCl (5 mL) was refluxed for 1 h. The progress of above reaction was checked by TLC. Upon completion, the reaction mixture was brought down to room temperature and solvent was evaporated under vacuum. The residue obtained was diluted with water (5 mL) and extracted in dichloromethane (3×5 mL). The combined organic layers were dried on Na_2SO_4 , filtered,

and concentrated under reduced pressure. The crude product was then purified through silica-gel chromatography using EtOAc:hexane (1:4) as an eluent to give functionalized 2-tetralone **11**.

2.3. Computational Details

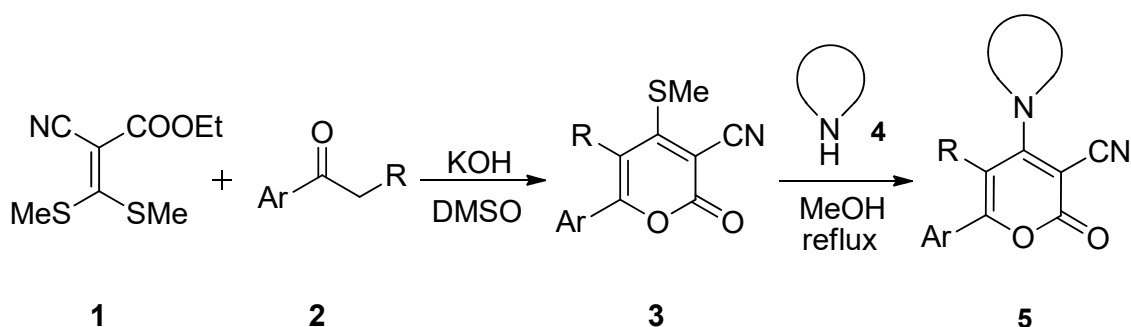
In order to study the title compounds, quantum mechanical calculations and molecular dynamics simulations have been performed by employing the programs from Schrödinger Materials Science Suite 2020-3 (SMSS). Quantum mechanical calculations were based on the DFT approach, and for these purposes, Jaguar [25–27] program was used for all DFT calculations. MD simulations were based on the OPLS3e force field [28–31], and for these purposes, the Desmond [32,33] program was used.

DFT calculations were done with combination of B3LYP [34–37] and CAM-B3LYP [38] exchange-correlation functionals, together with 6-31G(d,p), 6-311G(d,p) and 6-311++G(d,p) basis sets. B3LYP functional and 6-31G(d,p) basis set was used for geometrical optimizations of all molecules, followed by the vibrational analysis to check that the true ground states had been reached. In all cases, the vibrational analysis yielded only positive frequencies. Properties such as molecular electrostatic potential (MEP) and average local ionization energy (ALIE) have been calculated at the same level of theory by single-point energy calculations. Improved accuracy for self-consistent field procedure and grids was used. B3LYP/6-311G(d,p) level of theory was used for calculations of bond dissociation energy for hydrogen abstraction (H-BDE), while the simulation of UV spectra and analysis of excitations have been performed thanks to a time-dependent DFT (TD-DFT) approach at CAM-B3LYP/6-311++G(d,p) level of theory. To identify the molecular sites responsible for light absorption, natural transition orbital (NTO) formalism has been used [39].

For MD simulations, simulation time was set to 10 ns, while other parameters included a temperature of 300 K, normal pressure, and cut-off radius equal to 10 Å. In these simulations, the solvent was treated by a simple point charge (SPC) model [40]. After the MD simulations were performed, a simulation quality analysis was performed in order to assure that the selected MD parameters yielded reliable results.

3. Results and Discussions

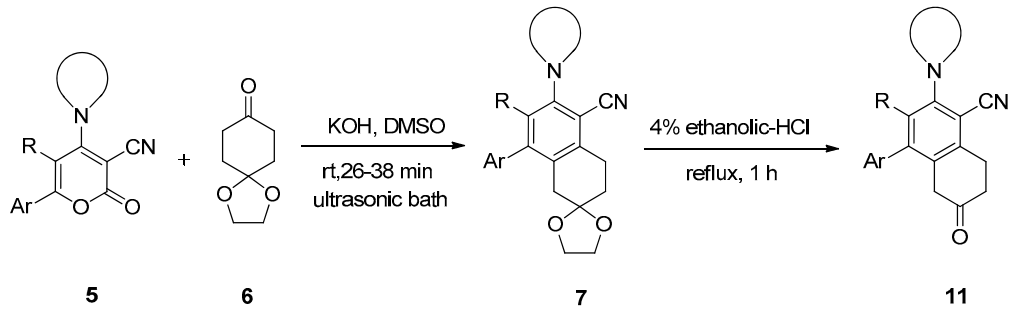
It has been found that 2*H*-pyran-2-ones are interesting scaffolds for the synthesis of functionally diverse aromatic and heteroaromatic systems with amazing photophysical and biological properties [41–49]. They are highly stable and prepared from easily accessible starting materials in excellent yields. The synthetic route towards the preparation of 2*H*-pyran-2-ones **3** involves KOH-mediated reaction of ethyl 2-cyano-3,3-dimethylsulfanylacrylate **1** with aromatic ketones **2** in DMSO [50,51]. Furthermore, methylsulfanyl groups containing 2-pyranones **3** were transformed into 6-aryl-2-oxo-4-amino-2*H*-pyran-3-carbonitriles **5** by treating with different secondary amines **4** under refluxing conditions (Scheme 1) [50,51]. The starting material **1** was easily obtained by reacting ethyl cyanoacetate with carbon disulphide and dimethyl sulphate in presence of freshly prepared sodium methoxide in absolute methanol [50,51].



Scheme 1. Synthesis of 2*H*-pyran-2-one precursors **3** and **5**.

Using 2*H*-pyran-2-ones **5** as synthons, we recently reported synthesis of highly functionalized spirocyclic ketals **7** through carbanion-induced ring transformation of 2*H*-pyran-2-ones **5** with 1,4-cyclohexanedione monoethylene ketal under ultrasound irradiation condition [52]. Furthermore, hydrolysis of ketals **7** with 4% ethanolic-HCl under refluxing condition produced 2-tetralones **11** in high yields (Table 1).

Table 1. Synthesis of spirocyclic ketals **7** and 2-tetralones **11**.



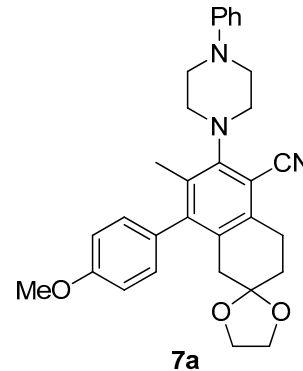
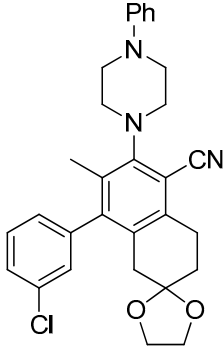
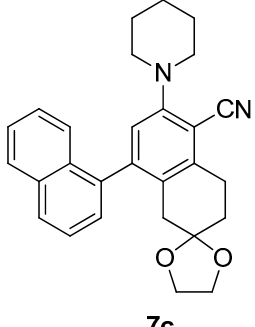
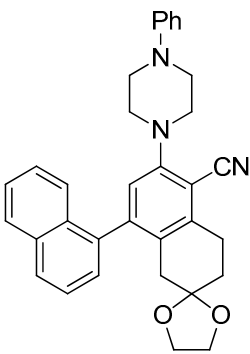
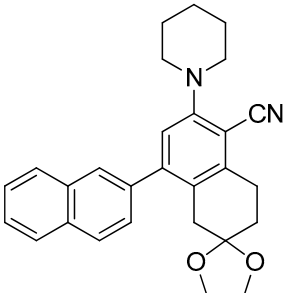
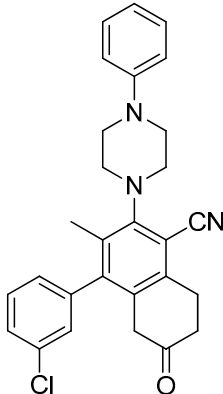
Entry	Structure 7/11	Time (min)	Yield (%)
RS-1	 <p>7a</p>	37	75
RS-2	 <p>7b</p>	35	82
RS-3	 <p>7c</p>	26	82

Table 1. Cont.

Entry	Structure 7/11	Time (min)	Yield (%)
RS-4	 <p style="text-align: center;">7d</p>	38	79
RS-5	 <p style="text-align: center;">7e</p>	32	80
RS-6	 <p style="text-align: center;">11</p>	60	84

3.1. Local Reactivity Properties—MEP and ALIE Surfaces

Fundamental parameters related to the reactivity, such as MEP and ALIE, have proven to be amongst the most important quantum molecular descriptors. They are fundamental since they are tightly connected to the electron density, a fundamental quantity within the DFT approach. Thanks to these descriptors, one can predict and analyze the local reactivity properties, i.e., to identify the most reactive molecular sites.

If the polarization and the nuclear rearrangement effects as a consequence of presence of a unit test charge at distance r are neglected, the equation for calculation of MEP ($V(r)$) can be written in the following form:

$$V(\vec{r}) = \sum \frac{Z_A}{|\vec{R}_A - \vec{r}|} - \int \frac{\rho(\vec{r}')}{|\vec{r}' - \vec{r}|} d\vec{r}' \quad (1)$$

In Equation (1), summation is performed over all nuclei. $\rho(r')$ denotes the electron density of a molecule, while $V(r)$ denotes the potential exerted at coordinate r .

According to Murray et al., ALIE is defined as a sum of orbital energies weighted by the orbital densities. With this being stated, ALIE can be calculated according to the following equation:

$$I(r) = \sum_i \frac{\rho_i(\vec{r})|\varepsilon_i|}{\rho(\vec{r})} \quad (2)$$

In Equation (2) electronic density of the i -th orbital at the point \vec{r} is denoted as $\rho_i(\vec{r})$, while the ε_i and $\rho_i(\vec{r})$ denote the orbital energy and total electronic density respectively.

From the aspect of visualization, these descriptors are most frequently presented by mapping their values on the electron density surface, which has been done in this work as well, taking into account the isosurface value of 0.001. MEP and ALIE surfaces of all studied molecules in this work have been presented in Figure 1.

While MEP quantity resembles the charge distribution with the studied molecules, ALIE quantity shows molecular sites where electrons are least tightly bonded. This means that the MEP surface indicates the molecular sites that are abundant or deficient with electrons, showing where the molecule is susceptible to electrostatic interactions with other molecules. On the other side, ALIE indicates where it is the easiest to remove an electron, therefore revealing the molecular sites that are sensitive towards electrophilic attacks.

In terms of charge distribution, MEP surfaces presented in Figure 1 indicate that the lowest MEP value is practically the same for all but one of the derivatives investigated in this work. Namely, the lowest MEP value of the RS-6 derivative is characterized by the value which is 5 kcal/mol lower than the other lowest MEP values, designating it as a derivative that is the least susceptible to interactions with electron-deficient molecular sites. On the other side, the same derivative has the highest value of MEP quantity, designating it as a derivative that could be the most sensitive towards the electron abundant molecular sites of other molecules. In general, the distribution of maximal and minimal MEP values is practically the same for all derivatives. The minimal MEP value has been always calculated for nitrogen atom; however, besides this molecular site, locations above benzene rings in all cases were also characterized by the lowest ALIE values. Therefore, these molecular sites are designated as being sensitive towards electrophilic attacks. The lowest ALIE value of 184.26 kcal/mol has been calculated for the RS-4 derivative, which is 7 kcal/mol lower than in the case of RS-2 derivative. In general, RS-1 and RS-2 are grouped around the value of 192 kcal/mol, while derivatives RS-3 to RS-6 are grouped around the value of 185 kcal/mol.

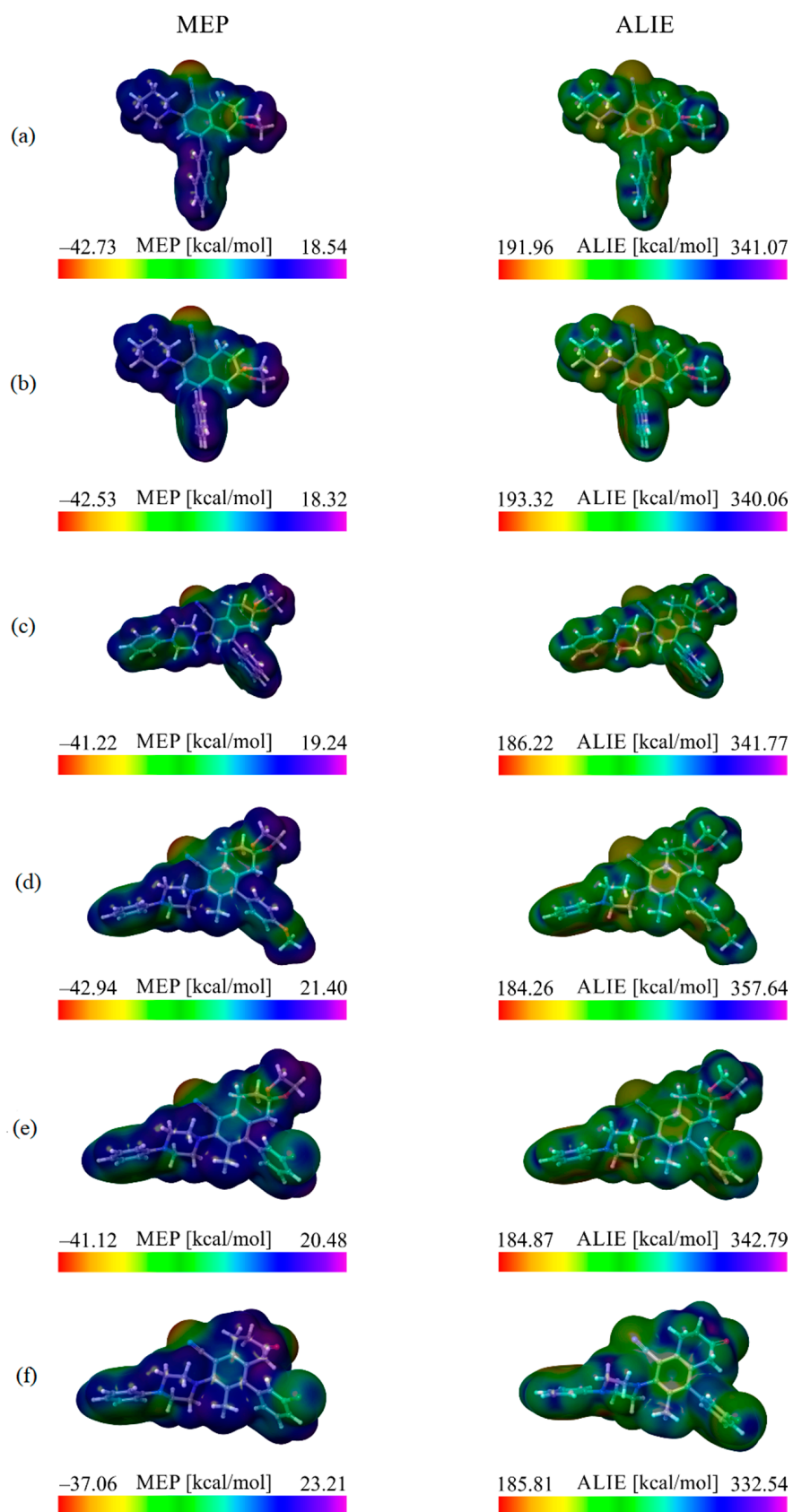


Figure 1. MEP and ALIE surfaces of (a) RS-1, (b) RS-2, (c) E-HLS3, (d) RS-4, (e) RS-5, and (f) RS-6 molecules.

3.2. Sensitivity towards Autoxidation

The stability of active components in the pharmaceutical formulations is one of the main concerns during the development of novel drugs. This type of stability is greatly influenced by the autoxidation mechanism, which might lead to the generation of genotoxic impurities [53,54], which do not just limit the overall applicability but also threaten the health. In terms of experimental activities, the identification of molecules prone to the autoxidation mechanism is tedious and time-consuming processes. Fortunately, it has been concluded that the sensitivity towards autoxidation is closely related to the H-BDE parameter, which allows scientists to predict sensitivity towards this important mechanism employing computational analysis. If some bonds are characterized by the H-BDE values in the range between 70 kcal/mol and 85 kcal/mol [55,56], then such molecular site is most probably susceptible to the autoxidation mechanism. The most important H-BDE values of all studied molecules have been summarized in Figure 2.

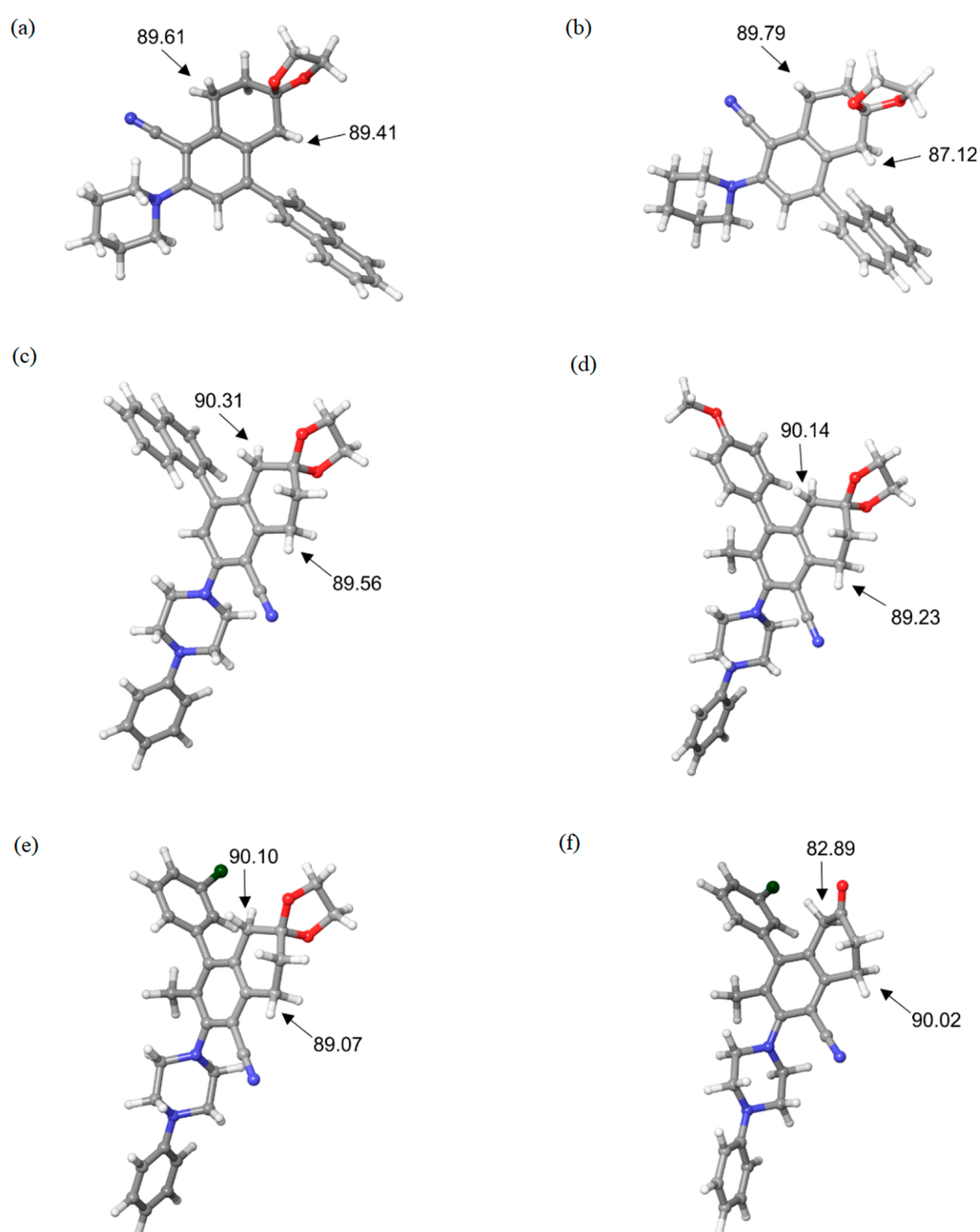


Figure 2. Selected H-BDE values of (a) RS-1, (b) RS-2, (c) RS-3, (d) RS-4, (e) RS-5, and (f) RS-6 molecules.

Figure 2 contains only H-BDE values that are close to the border threshold. All other H-BDE values are much higher than the defined threshold and are therefore not significant for further discussion. Results presented in Figure 2 indicate that only one derivative violates the criteria for autoxidation, with respect to the upper border value of H-BDE. This derivative is denoted as RS-6 and is characterized by one H-BDE value equal to ~ 83 kcal/mol. This is certainly below the upper border level of 85 kcal/mol, meaning that it could be susceptible to autoxidation and produce genotoxic impurities during the shelf storage. On the other side, all other molecules are characterized by the H-BDE values higher than the upper threshold, indicating that they should be stable during the storage. Gathered results regarding H-BDE values indicate that all but one of the derivatives (RS-6) have suitable values of H-BDE, indicating stability with respect to the autoxidation mechanism.

3.3. Interactions with Water

In this work, MD simulations were used to investigate the reactivity of title compounds with water molecules, which is one of the most important aspects of the pharmaceutical potential of the mentioned molecules. For these purposes, MD simulations are important because they allow one to explicitly involve water molecules and investigate rather large systems that would be impossible to treat with quantum-mechanical calculations.

In our MD simulations, for each studied molecule, we have run a separate MD simulation on a simulation box that consists of that molecule surrounded by approximately 2500 water molecules. For these purposes, a System Builder tool SMSS was used. The number of added water molecules was controlled by varying the dimensions of a cubic simulation box. Other MD details were as described in the Computational Details section. Simulation boxes were cubic.

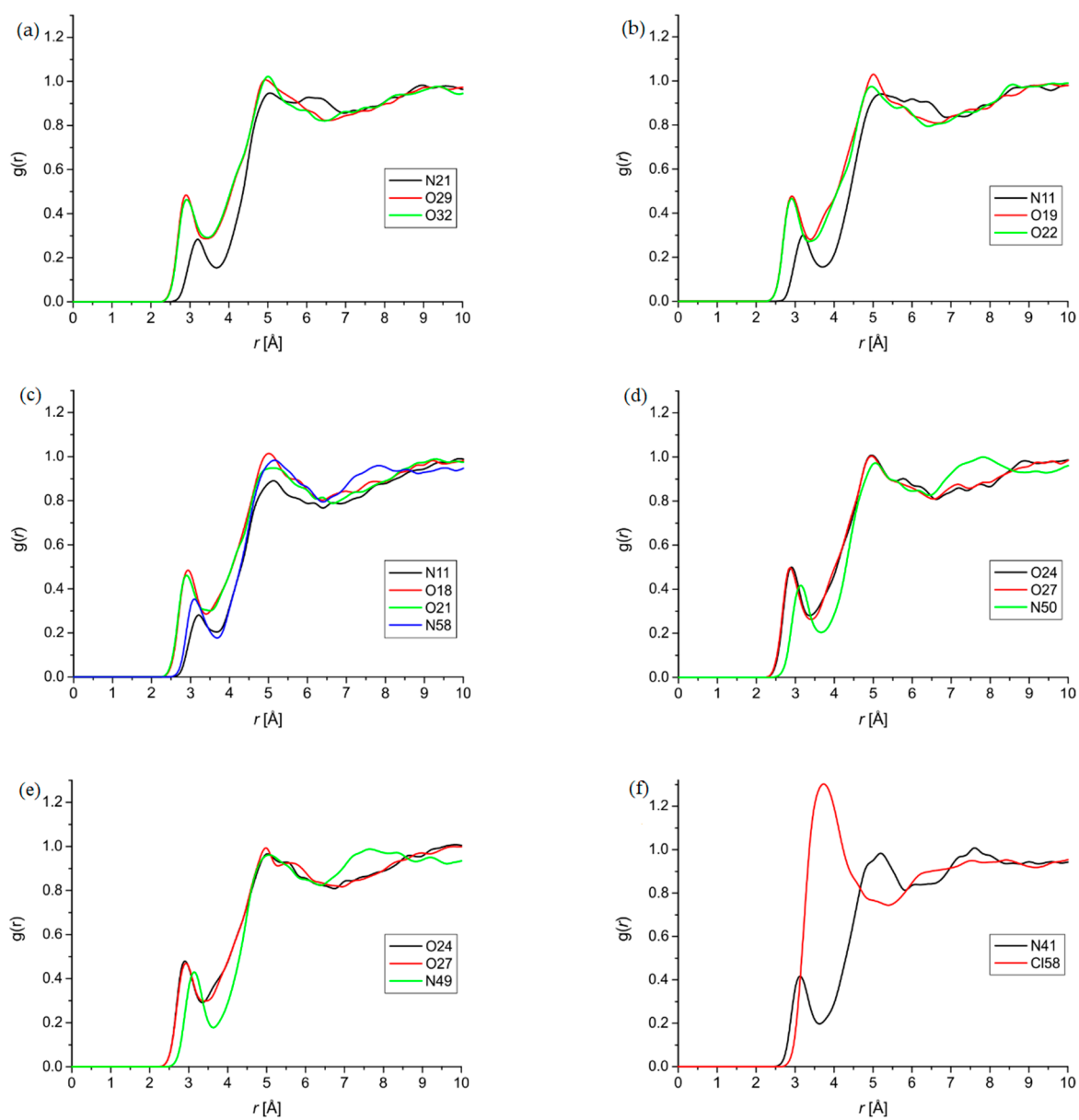
Interactions with water were studied both globally, through calculations of interaction energy and an average number of the hydrogen bonds between selected molecule and water (Table 2), and locally through calculations of radial distribution functions (RDF) which indicate the atoms of molecules with the pronounced interactions with water (Figure 3).

For each MD frame, interaction energy has been calculated by subtracting the total energies of selected molecule and solvent, from the total energy of the molecule + solvent system. Then, the interaction energy was averaged over all frames. According to the interaction energies with water, presented in Table 2, it can be seen that there is a significant difference between studied molecules in the extent to which they interact with water. The magnitude of this parameter took values in the range between 63 kcal/mol to almost 77 kcal/mol. The lowest interaction energies with water have been calculated for RS-1, RS-2, and RS-6 molecules, while RS-3 and RS-4 molecules were characterized by the strongest interactions with water. RS-5 molecule was somewhere between, with the magnitude of interaction energy equal to ~ 70 kcal/mol. It was interesting also to note that all but one derivative on average formed ~ 3 hydrogen bonds with water molecules. The only exclusion was the RS-4 molecule, which formed more than 4 hydrogen bonds with water molecules on average, which explains why this molecule had the highest interaction energies with water. In order to investigate the local reactivity of studied molecules with water, we have calculated the RDFs. The most representative RDFs are presented in Figure 3.

Results presented in Figure 3 indicate the absence of atoms that have significant interactions with water molecules, since all $g(r)$ curves are characterized by the low $g(r)$ values whose maximal values are located at high distances, well above the 2 Å. Additionally, although the studied molecules are relatively large, it has been observed that all of them have only 2–4 atoms with RDFs worth of mentioning when the size and profile of $g(r)$ curves are taken into account. In all cases, nitrogen and oxygen were identified as the ones with relatively important RDFs, with the small exception of the chlorine atom in the case of the RS6 molecule. It is also worthy of mentioning that the RS4 molecule, characterized by the highest interaction energy with water is characterized by the three relatively decent RDFs, belonging to two oxygen and one nitrogen atoms.

Table 2. Interaction energies between studied molecules and water, with the average number of the formed hydrogen bonds with water.

Molecules	Interaction Energy [kcal/mol]	Average Number of Hydrogen Bonds
RS-1	−65.175	3.020
RS-2	−63.523	3.024
RS-3	−75.854	3.019
RS-4	−76.809	4.057
RS-5	−70.066	3.127
RS-6	−66.056	2.925

**Figure 3.** RDFs of (a) RS1, (b) RS2, (c) RS3, (d) RS4, (e) RS5, and (f) RS6 molecules.

3.4. Identification of Suitable Excipients

Improvement of stabilization, solubility, delivery, and other properties is another important challenge during the development of novel pharmaceutical formulations, once the suitable active components are identified. To achieve this, it is necessary to combine active components with compounds, called excipients that have suitable properties. Since there is no universal excipient, it is necessary to select one.

The selection of suitable excipient might be a tedious and time-consuming process; however, thanks to the MD simulations, the selection of adequate excipient can be significantly narrowed. The key goal in the identification of suitable excipient is to identify the one which is compatible with the active component in terms of solubility parameters. If they have similar values of the solubility parameter, then they are compatible and can be combined in a novel pharmaceutical formulation [57–59].

For these purposes, the solubility parameter can be calculated by using the MD simulations and by applying the following Equation (3):

$$\delta = \sqrt{\frac{\Delta H_V - RT}{V_m}} \quad (3)$$

where ΔH_V denotes heat of vaporization and V_m denotes the molar volume. In order to calculate the solubility parameter for all studied compounds, for each compound separate MD simulation was performed, on the cubic box containing 32 such molecules. All other parameters were the same as mentioned in the Computational Details section. Additionally, the solubility parameters were calculated for the frequently used excipients, to be able to compare the solubility parameters of studied compounds and identify which type of excipient could be potentially suitable. Frequently used excipients studied in this work were polyvinylpyrrolidone polymer (PVP), maltose, and sorbitol. Solubility parameters of RS1-6 molecules and frequently used excipients are summarized in Table 3.

Table 3. Values of solubility parameters δ [MPa^{1/2}] for studied compounds and frequently used excipients.

Molecules	δ [MPa ^{1/2}]
RS1	18.825
RS2	18.663
RS3	19.397
RS4	19.264
RS5	19.021
RS6	19.513
PVP	18.515
Maltose	28.564
Sorbitol	32.425

Results presented in Table 3 indicate that all studied molecules in this work have rather similar values, ranging between 18.6 and 19.5, indicating that modifications do not cause significant changes in this parameter. Additionally, by comparing the solubility parameters of frequently used excipients, it is evident that the PVP excipient is the most compatible with studied compounds. Namely, the solubility parameters of studied compounds are very similar to that of PVP, indicating that this compound could be potentially practically applied for the development of novel pharmaceutical formulations based on studied derivatives.

4. Conclusions

In summary, the DFT calculations were used to identify the molecular sites prone to electrostatic interactions with other molecules by MEP surfaces, while ALIE surfaces were used to identify the molecular sites sensitive to the electrophilic attacks. It has been shown by our calculations that the nitrogen atom is crucial for the characteristic MEP surface, while the lowest ALIE values have been identified above benzene rings as well. H-BDE values indicated that one of the studied compounds, namely the RS6 molecule, dangerously violates the upper border threshold of 85 kcal/mol, meaning that potentially genotoxic impurities could be formed in case of the formulation based on this derivative. All other derivatives seem to be stable towards the autoxidation mechanism. Furthermore, MD simulations indicated that, of all studied molecules, RS4 is characterized by the highest interaction energies with water, and at the same time, this molecule is characterized by the highest number of hydrogen bonds formed between the observed molecule and water molecules. RDFs did not indicate that any of the atoms of studied compounds have particularly strong interactions with water molecules since there were no $g(r)$ curves characterized by the highest $g(r)$ values at distances of around 2 Å. MD simulations also helped in identifying which frequently used excipient could be used in the case of title compounds. Namely, the calculations of solubility parameters indicated that the studied compounds could be highly compatible with the PVP excipient, as their solubility parameters are very similar.

Author Contributions: Conceptualization, S.E.S. and F.V.S.; methodology, S.E.S., R.R.P., K.T. and F.V.S.; software, S.J.A. and S.A.; validation, C.S. and R.G.A.; formal analysis, S.E.S. and S.P.K.; investigation, S.E.S. and F.V.S.; resources, F.V.S., S.J.A. and S.A.; data curation, R.R.P., A.S., A.M.E. and A.H.B.; writing—original draft preparation, S.E.S.; writing—review and editing, F.V.S. and S.P.K.; visualization, C.S. and R.G.A.; supervision, F.V.S.; project administration, S.P.K.; funding acquisition, A.S., A.M.E. and A.H.B. All authors have read and agreed to the published version of the manuscript.

Funding: This research was funded by the researchers' supporting project number (RSP-2021/15), King Saud University, Riyadh, Saudi Arabia.

Institutional Review Board Statement: Not applicable.

Informed Consent Statement: Not applicable.

Data Availability Statement: Not applicable.

Acknowledgments: Authors thankfully acknowledge VIT, Vellore for providing analytical facilities. SPK is thankful to the Director, Amrita Vishwa Vidyapeetham, Mysuru Campus, Mysuru for providing infrastructural supports. The authors acknowledge the financial support of the Ministry of Education, Science, and Technological Development of the Republic of Serbia (Grant No. 451-03-68/2020-14/200125). The authors extend their appreciation to the researchers' supporting project number (RSP-2021/15), King Saud University, Riyadh, Saudi Arabia.

Conflicts of Interest: The authors declare no potential conflict of interest in publishing this work.

References

1. Silveira, C.C.; Braga, A.; Kaufman, T.; Lenardao, E.J. Synthetic approaches to 2-tetralones. *Tetrahedron* **2004**, *60*, 8295–8328. [[CrossRef](#)]
2. Makhey, D.; Li, D.; Zhao, B.; Sim, S.-P.; Li, T.-K.; Liu, A.; Liu, L.F.; LaVoie, E.J. Substituted Benzo[*i*]phenanthridines as Mammalian Topoisomerase-Targeting Agents. *Bioorg. Med. Chem.* **2003**, *11*, 1809–1820. [[CrossRef](#)]
3. El Sayed, K.A.; Foudah, A.I.; Mayer, A.M.S.; Crider, A.M.; Song, D. Synthesis, microbial transformation, and pharmacological evaluation of 4,5-dihydronaphtho[2,1-*b*]furan-2-ones and related analogues. *MedChemComm* **2013**, *4*, 1231–1238. [[CrossRef](#)]
4. Pautigny, C.; Debouit, C.; Vayron, P.; Ayad, T.; Ratovelomanana-Vidal, V. Ratovelomanana-Vidal, Asymmetric hydrogenation of trisubstituted-*N*-acetyl enamides derived from 2-tetralones using ruthenium-SYNPHOS catalysts: A practical synthetic approach to the preparation of β 3-adrenergic agonist SR58611A. *Tetrahedron Asymmetry* **2010**, *21*, 1382–1388. [[CrossRef](#)]
5. Balijapalli, U.; Udayadasan, S.; Shanmugam, E.; Iyer, S.K. Synthesis, photophysical and acidochromic properties of a series of tetrahydrodibenzo[*a,i*]phenanthridine chromophores. *Dye Pigment.* **2016**, *130*, 233–244. [[CrossRef](#)]
6. Umamahesh, B.; Sathiskumar, U.; Augustine, G.; Easwaramoorthi, S.; Ayyadurai, N.; Sathiyarayanan, K.I. Photophysical studies of donor, acceptor substituted tetrahydrodibenzo[*a,i*]phenanthridines. *Dye. Pigment.* **2016**, *134*, 409–418. [[CrossRef](#)]

7. Ponram, M.; Balijapalli, U.; Sambath, B.; Iyer, S.K.; Venkatachalapathy, B.; Cingaram, R.; Sundaramurthy, K.N. Development of paper-based chemosensor for the detection of mercury ions using mono- and tetra-sulfur bearing phenanthridines. *New J. Chem.* **2018**, *42*, 8530–8536. [CrossRef]
8. Muthukumar, V.; Iyer, S.K. Highly selective chemosensor for the detection of Ru³⁺ ion by fluorescent turn-on response and its bioimaging recognition in living cells. *Sens. Actuators B* **2018**, *267*, 373–380.
9. Goel, A.; Sharma, A.; Rawat, M.; Anand, R.S.; Kant, R. Synthesis of Fluorescent C2-Bridged Teraryls and Quateraryls for Blue, Sky-Blue, and Green Color Light-Emitting Devices. *J. Org. Chem.* **2014**, *79*, 10873–10880. [CrossRef]
10. Wang, B.; Peng, F.; Huang, W.; Zhou, J.; Zhang, N.; Sheng, J.; Haruehanroengra, P.; He, G.; Han, B. Rational drug design, synthesis, and biological evaluation of novel chiral tetrahydronaphthalene-fused spirooxindole as MDM2-CDK4 dual inhibitor against glioblastoma. *Acta Pharm. Sin. B* **2020**, *10*, 1492–1510. [CrossRef]
11. Ates-Alagoz, Z.; Yildiz, S.; Buyukbingol, E. Antimicrobial Activities of Some Tetrahydronaphthalene-Benzimidazole Derivatives. *Chemotherapy* **2007**, *53*, 110–113. [CrossRef]
12. Uppal, A.; Kothiyal, P.; Singh, A. Hybrid Class Phenylthiazole and 1,2,3,4-Tetrahydronaphthalene Target Sertraline Transporter for Antidepressant Action Revealed by Molecular Docking Studies. *J. Heterocycl. Chem.* **2015**, *52*, 1429–1437. [CrossRef]
13. Barker, M.; Clackers, M.; Copley, R.; Demaine, D.A.; Humphreys, D.; Inglis, G.G.A.; Johnston, M.J.; Jones, H.T.; Haase, M.V.; House, D.; et al. Dissociated Nonsteroidal Glucocorticoid Receptor Modulators; Discovery of the Agonist Trigger in a Tetrahydronaphthalene-Benzoxazine Series. *J. Med. Chem.* **2006**, *49*, 4216–4231. [CrossRef] [PubMed]
14. Rho, Y.S.; Ko, H.K.; Sin, H.; Yoo, D.J. A Facile Total Synthesis of Idarubicinone. *Bull. Kor. Chem. Soc.* **1999**, *20*, 1517–1520.
15. Hauser, F.M.; Prasanna, S. Total syntheses of (+,−)-duanomycinone. Regiospecific preparations of (+,−)-7,9-dideoxydaunomycinone and 6,11-dihydroxy-4-methoxy-7,8,9,10-tetrahydronaphthacene-5,9,12-trione. *J. Am. Chem. Soc.* **1981**, *103*, 6378–6386. [CrossRef]
16. Franco, T.; Silvana, F. A process for the Preparation of Nepinalone. European Patent AppIEP0507001A1, 7 October 1992.
17. Cogley, C.J.; Evans, G.; Fanjul, T.; Simmonds, S.; Woods, A. New catalytic route for the synthesis of an optically active tetralone-derived amine for rotigotine. *Tetrahedron Lett.* **2016**, *57*, 986–989. [CrossRef]
18. Batra, H.; Tuladhar, S.M. An Improved Process to Prepare Treprostinil, the Active Ingredient in Remodulin®. WO 2009/078965, 25 June 2009. Available online: <https://patentscope.wipo.int/search/en/detail.jsf?docId=WO2009078965> (accessed on 18 June 2021).
19. Aminpour, M.; Montemagno, C.; Tuszyński, J.A. An overview of molecular modelling for drug discovery with specific illustrative examples of applications. *Molecules* **2019**, *24*, 1693. [CrossRef]
20. Thomas, R.; Mary, Y.S.; Resmi, K.S.; Narayana, B.; Sarojini, S.B.K.; Armaković, S.; Armaković, S.J.; Vijayakumar, G.; van Alsenoy, C.; Mohan, B.J. Synthesis and spectroscopic study of two new pyrazole derivatives with detailed computational evaluation of their reactivity and pharmaceutical potential. *J. Mol. Struct.* **2019**, *1181*, 599–612. [CrossRef]
21. Beegum, S.; Mary, Y.S.; Thomas, R.; Armaković, S.; Armaković, S.J.; Zitko, J.; Dolezal, M.; Van Alsenoy, C. Exploring the detailed spectroscopic characteristics, chemical and biological activity of two cyanopyrazine-2-carboxamide derivatives using experimental and theoretical tools. *Spectrochim. Acta Part A: Mol. Biomol. Spectrosc.* **2020**, *224*, 117414. [CrossRef] [PubMed]
22. Zainuri, D.A.; Arshad, S.; Khalib, N.C.; Razak, I.A.; Pillai, R.R.; Sulaiman, S.F.; Hashim, N.S.; Ooi, K.L.; Armaković, S.; Armaković, S.J. Synthesis, XRD crystal structure, spectroscopic characterization (FT-IR, 1H and 13C NMR), DFT studies, chemical reactivity and bond dissociation energy studies using molecular dynamics simulations and evaluation of antimicrobial and antioxidant activities of a novel chalcone derivative, (E)-1-(4-bromophenyl)-3-(4-iodophenyl) prop-2-en-1-one. *J. Mol. Struct.* **2017**, *1128*, 520–533.
23. Mary, Y.S.; Aswathy, V.V.; Panicker, C.Y.; Bielenica, A.; Brzózka, P.; Savchenko, O.; Armaković, S.; Armaković, S.J.; Van Alsenoy, C. Spectroscopic, single crystal XRD structure, DFT and molecular dynamics investigation of 1-(3-chloro-4-fluorophenyl)-3-[3-(trifluoromethyl)phenyl]thiourea. *RSC Adv.* **2016**, *6*, 111997–112015. [CrossRef]
24. Pillai, R.R.; Karrouchi, K.; Fettach, S.; Armaković, S.; Armaković, S.; Brik, Y.; Taoufik, J.; Radi, S.; Faouzi, M.E.A.; Ansar, M. Synthesis, spectroscopic characterization, reactive properties by DFT calculations, molecular dynamics simulations and biological evaluation of Schiff bases tethered 1,2,4-triazole and pyrazole rings. *J. Mol. Struct.* **2019**, *1177*, 47–54. [CrossRef]
25. Bochevarov, A.D.; Harder, E.; Hughes, T.F.; Greenwood, J.R.; Braden, D.A.; Philipp, D.M.; Rinaldo, D.; Halls, M.; Zhang, J.; Friesner, R.A. Jaguar: A high-performance quantum chemistry software program with strengths in life and materials sciences. *Int. J. Quantum Chem.* **2013**, *113*, 2110–2142. [CrossRef]
26. Jacobson, L.D.; Bochevarov, A.D.; Watson, M.A.; Hughes, T.F.; Rinaldo, D.; Ehrlich, S.; Steinbrecher, T.B.; Vaitheeswaran, S.; Philipp, D.M.; Halls, M.D.; et al. Automated Transition State Search and Its Application to Diverse Types of Organic Reactions. *J. Chem. Theory Comput.* **2017**, *13*, 5780–5797. [CrossRef] [PubMed]
27. Schrödinger Release 2020-3: Jaguar, Schrödinger, LLC: New York, NY, USA, 2020; Available online: <https://www.schrodinger.com/products/jaguar> (accessed on 18 June 2021).
28. Harder, E.; Damm, W.; Maple, J.; Wu, C.; Reboul, M.; Xiang, J.Y.; Wang, L.; Lupyan, D.; Dahlgren, M.K.; Knight, J.L.; et al. OPLS3: A Force Field Providing Broad Coverage of Drug-like Small Molecules and Proteins. *J. Chem. Theory Comput.* **2016**, *12*, 281–296. [CrossRef]
29. Shivakumar, D.; Williams, J.; Wu, Y.; Damm, W.; Shelley, J.; Sherman, W. Prediction of Absolute Solvation Free Energies using Molecular Dynamics Free Energy Perturbation and the OPLS Force Field. *J. Chem. Theory Comput.* **2010**, *6*, 1509–1519. [CrossRef]

30. Jorgensen, W.L.; Maxwell, D.S.; Tirado-Rives, J. Development and Testing of the OPLS All-Atom Force Field on Conformational Energetics and Properties of Organic Liquids. *J. Am. Chem. Soc.* **1996**, *118*, 11225–11236. [[CrossRef](#)]
31. Jorgensen, W.L.; Tirado-Rives, J. The OPLS [optimized potentials for liquid simulations] potential functions for proteins, energy minimizations for crystals of cyclic peptides and crambin. *J. Am. Chem. Soc.* **1988**, *110*, 1657–1666. [[CrossRef](#)] [[PubMed](#)]
32. Bowers, K.J.; Chow, D.E.; Xu, H.; Dror, R.O.; Eastwood, M.P.; Gregersen, B.A.; Klepeis, J.L.; Kolossvary, I.; Moraes, M.A.; Sacerdoti, F.D. Scalable algorithms for molecular dynamics simulations on commodity clusters. In Proceedings of the SC'06 Proc. 2006 ACM/IEEE Conf. Supercomput, Tampa, FL, USA, 11–17 November 2006; p. 43.
33. *Schrödinger Release 2020-3: Desmond Molecular Dynamics System*; D. E. Shaw Research: New York, NY, USA, 2020.
34. Becke, A.D. Density-functional thermochemistry. III. The role of exact exchange. *J. Chem. Phys.* **1993**, *98*, 5648–5652. [[CrossRef](#)]
35. Lee, C.; Yang, W.; Parr, R.G. Development of the Colle-Salvetti correlation-energy formula into a functional of the electron density. *Phys. Rev. B* **1988**, *37*, 785. [[CrossRef](#)] [[PubMed](#)]
36. Vosko, S.H.; Wilk, L.; Nusair, M. Accurate spin-dependent electron liquid correlation energies for local spin density calculations: A critical analysis. *Can. J. Phys.* **1980**, *58*, 1200–1211. [[CrossRef](#)]
37. Stephens, P.J.; Devlin, F.J.; Chabalowski, C.F.; Frisch, M.J. Ab Initio Calculation of Vibrational Absorption and Circular Dichroism Spectra Using Density Functional Force Fields. *J. Phys. Chem.* **1994**, *98*, 11623–11627. [[CrossRef](#)]
38. Yanai, T.; Tew, D.; Handy, N.C. A new hybrid exchange–correlation functional using the Coulomb-attenuating method (CAM-B3LYP). *Chem. Phys. Lett.* **2004**, *393*, 51–57. [[CrossRef](#)]
39. Martin, R.L. Natural transition orbitals. *J. Chem. Phys.* **2003**, *118*, 4775–4777. [[CrossRef](#)]
40. Berendsen, H.J.C.; Postma, J.P.M.; van Gunsteren, W.F.; Hermans, J. Interaction models for water in relation to protein hydration. *Int. Forces* **1981**, 331–342.
41. Goel, A.; Ram, V.J. Natural and synthetic 2H-pyran-2-ones and their versatility in organic synthesis. *Tetrahedron* **2009**, *65*, 7865–7913. [[CrossRef](#)]
42. Pratap, R.; Ram, V.J. 2H-Pyran-2-ones and their annelatedanalogs as multifaceted building blocks for the fabrication of diverse heterocycles. *Tetrahedron* **2017**, *73*, 2529–2590. [[CrossRef](#)]
43. Singh, F.V.; Kole, P.B. Metal-Free Synthesis of Biaryl- and Teraryl-Cored Diarylmethanes by Ring Transformation of 2H-Pyran-2-ones. *Synthesis* **2019**, *51*, 1435–1444. [[CrossRef](#)]
44. Shetgaonkar, S.E.; Singh, F.V. Ultrasound-assisted one pot synthesis of polysubstituted *meta*-terphenyls using ring transformation strategy. *Synth. Commun.* **2019**, *49*, 1092–1102. [[CrossRef](#)]
45. Kole, P.B.; Singh, F.V. Versatile Synthesis of Functionalized Tetrahydroisoquinolines by Ring Transformation of 2H-Pyran-2-ones. *Aust. J. Chem.* **2019**, *72*, 524. [[CrossRef](#)]
46. Shetgaonkar, S.E.; Singh, F.V. Base-mediated alternate route for multi-functionalized allylbenzenes using ring transformation strategy. *Synth. Commun.* **2020**, *50*, 2511–2521. [[CrossRef](#)]
47. Chandrasekar, S.; Singh, F.V. Metal-Free Synthesis of Thermally Stable Fluorescent *p*-Terphenyls by Ring Transformation of 2H-Pyran-2-ones. *ChemistrySelect* **2020**, *5*, 7452–7459. [[CrossRef](#)]
48. Kanimozhi, R.; Singh, F.V. Metal-free synthesis and characterization of 1,3-Bis(heteroaryl)benzenes followed by the photophysical studies using ultraviolet–visible and fluorescence spectroscopy. *J. Mol. Struct.* **2020**, *1219*, 128633. [[CrossRef](#)]
49. Chandrasekar, S.; Kennedy, L.J.; Singh, F.V. Synthesis, spectral characterization and photophysical studies of tetrahydroquinolines. *J. Mol. Struct.* **2020**, *1226*, 129365.
50. Tominaga, Y.; Ushiroguchi, A.; Matsuda, Y. Synthesis and reaction of 6-substituted 3-methoxycarbonyl-4-methylthio-2H-pyran-2-one derivatives. *J. Heterocycl. Chem.* **1987**, *24*, 1557–1567. [[CrossRef](#)]
51. Tominaga, Y. Synthesis of heterocyclic compounds using ketene dithioacetals. *Trends Heterocycl. Chem.* **1991**, *2*, 43. [[CrossRef](#)]
52. Shetgaonkar, S.E.; Singh, F.V. A Metal-Free Approach for the Synthesis of 2-Tetralones via Carbanion-Induced Ring Transformation of 2H-Pyran-2-ones. *Synthesis* **2018**, *50*, 3540–3548.
53. Andersson, T.; Broo, A.; Evertsson, E. Prediction of drug candidates' sensitivity toward autoxidation: Computational estimation of CH dissociation energies of carbon-centered radicals. *J. Pharm. Sci.* **2014**, *103*, 1949–1955. [[CrossRef](#)]
54. Raillard, S.P.; Bercu, J.; Baertschi, S.; Riley, C.M. Prediction of Drug Degradation Pathways leading to Structural Alerts for Potential Genotoxic Impurities. *Org. Process. Res. Dev.* **2010**, *14*, 1015–1020. [[CrossRef](#)]
55. Wright, J.S.; Shadnia, H.; Chepelev, L.L. Stability of carbon-centered radicals: Effect of functional groups on the energetics of addition of molecular oxygen. *J. Comput. Chem.* **2009**, *30*, 1016–1026. [[CrossRef](#)]
56. Gryn'Ova, G.; Hodgson, J.L.; Coote, M.L. Revising the mechanism of polymer autooxidation. *Org. Biomol. Chem.* **2010**, *9*, 480–490. [[CrossRef](#)]
57. Greenhalgh, D.J.; Williams, A.; Timmins, P.; York, P. Solubility parameters as predictors of miscibility in solid dispersions. *J. Pharm. Sci.* **1999**, *88*, 1182–1190. [[CrossRef](#)] [[PubMed](#)]
58. Rowe, R. Adhesion of film coatings to tablet surfaces—A theoretical approach based on solubility parameters. *Int. J. Pharm.* **1988**, *41*, 219–222. [[CrossRef](#)]
59. Rowe, R.C. Interactions in coloured powders and tablet formulations: A theoretical approach based on solubility parameters. *Int. J. Pharm.* **1989**, *53*, 47–51. [[CrossRef](#)]